STEREO/EUVI Science at LMSAL

Markus J. Aschwanden, Jean-Pierre Wuelser, D.Alexander,
S.Freeland, N.Hurlburt, J.Lemen, T.Metcalf, R.Nightingale, N.Nitta, J.Wolfson

Static 3D Reconstruction and Modeling

- Active Region Loops
- Quiescent filaments, prominences

Dynamic 3D Reconstruction and Modeling

- Dynamic loops, flare loops, postflare loops
- Eruptive filaments, prominences
- CME structures, coronal dimming

Technical and Methodical Issues

- Feature recognition, tiepoints vs. forward-fitting
- Spatial resolution, Pointing stability, ISS
- Aspect angle separation vs. optimum science
- SSW, Software Approach at LMSAL

You can access this presentation on the web:

http://diapason.lmsal.com/~aschwar

Quasi-Static EUV Structures

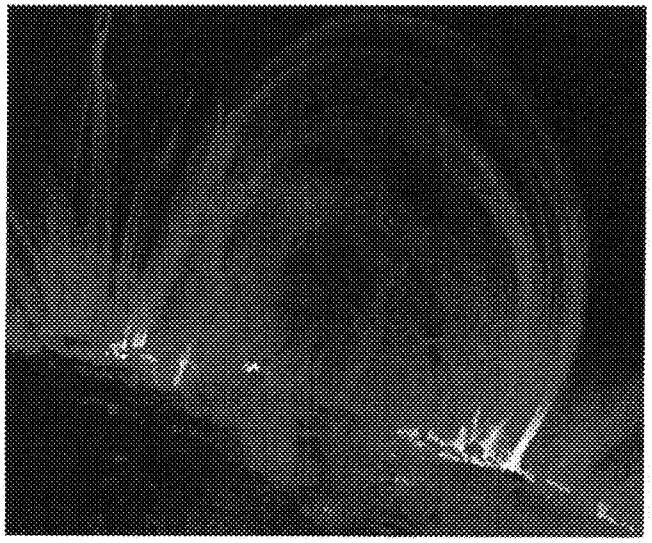

Active Region Loops:

This image of coronal loops over the eastern limb of the Sun was taken in the TRACE 171 A pass band, characteristic of plasma at 1 MK, on November 6, 1999, at 02:30 UT. A flare occurred about 8 hours earlier, possibly related to intense heating during an extended postflare phase. The image was rotated over +90 degrees.

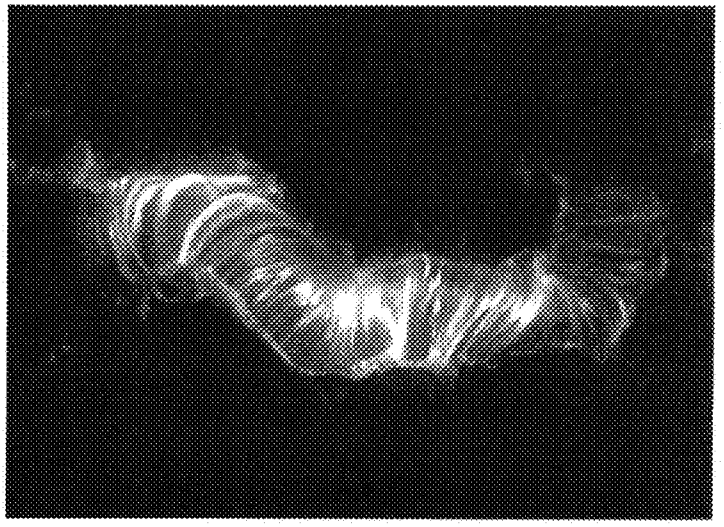

Postflare Loops:

A major solar flare produces an arcade resembling a slinky. The X5.7 flare occurred at 10:03UT on 14 July 2000, in Active Region 9077, observed by TRACE in its 195 A pass band. A filament in the center of the region destabilizes and is seen lifting off. Following this mass ejection, an arcade of magnetic fields lights up, cooling down from many millions of degress. This huge flare was also accompagnied by a geoeffective CME. The field of view is 230,000 by 170,000 km.

Automated Pattern Recognition

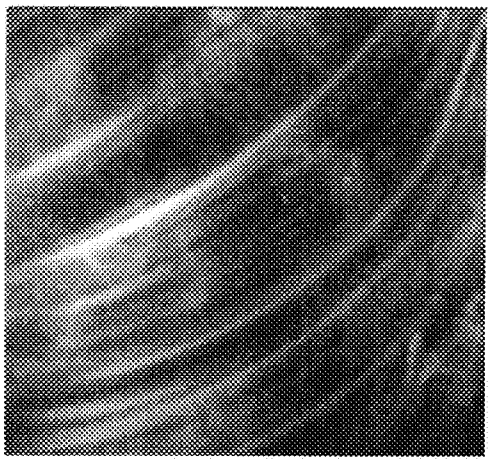

TRACE 195, 1998 Aug 25, 04:00 UT

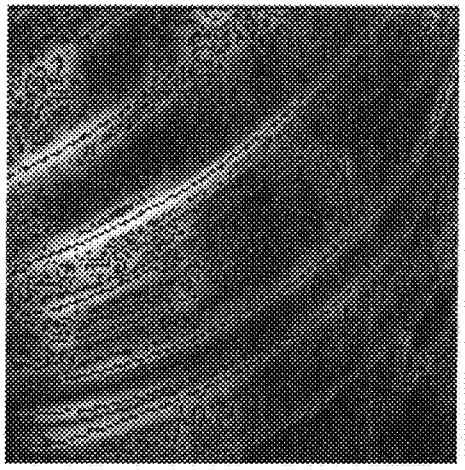

4-Gradient direction algorithm

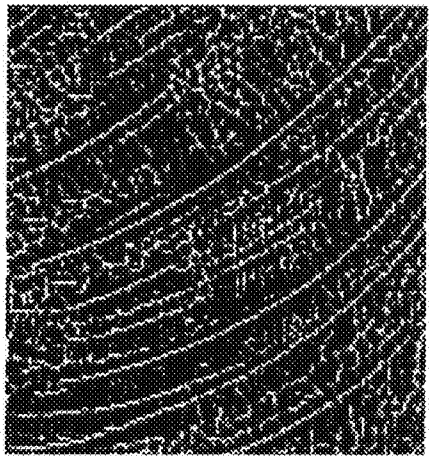

Local maximum criterion

Automated pattern recognition algorithms are more objective and efficient than human interaction, and can be trained for every morphological shape if a quantitative criterion can be defined.

Coronal loops can be traced by detection of linear structures (see algorithm of Louis Strous applied to TRACE images: http://louis.lmsal.com/~strous/cdaw.html).

Problems occur for intersecting structures, which can only be disentangled with help of calculated projections from 3D models.

3D-parametrization s(x,y,z)

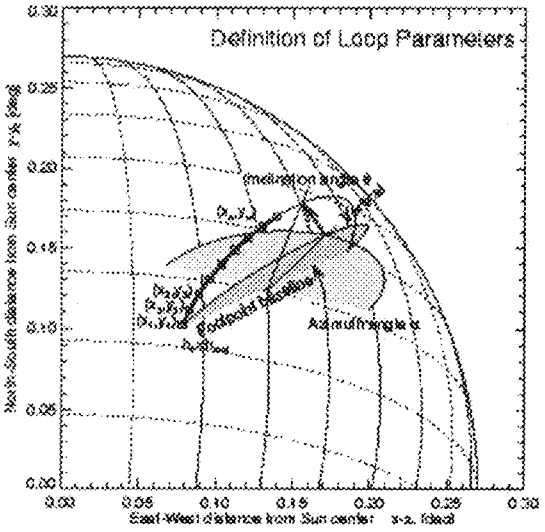

The coordinates of a one-dimensional feature (e.g. loop or filament) can be parameterized with a length coordinate s(x,y,z) as function of 3D cartesian coordinates (x,y,z), where (x,y) are measured in image plane of stereo image 1, while z represents a variable that is constrained by the projection s(x',y',z') onto the second stereoimage.

For n loops occurring along a line-of-sight over a height extent h, some a-priori constraints on the geometric loop shape (e.g. near-circular, near-elliptical) have to be defined that restrict the possible solution space to a height range of about dh=h/n .

Physical model from hydrostatic equations [n_e0, E_H0, s_H]

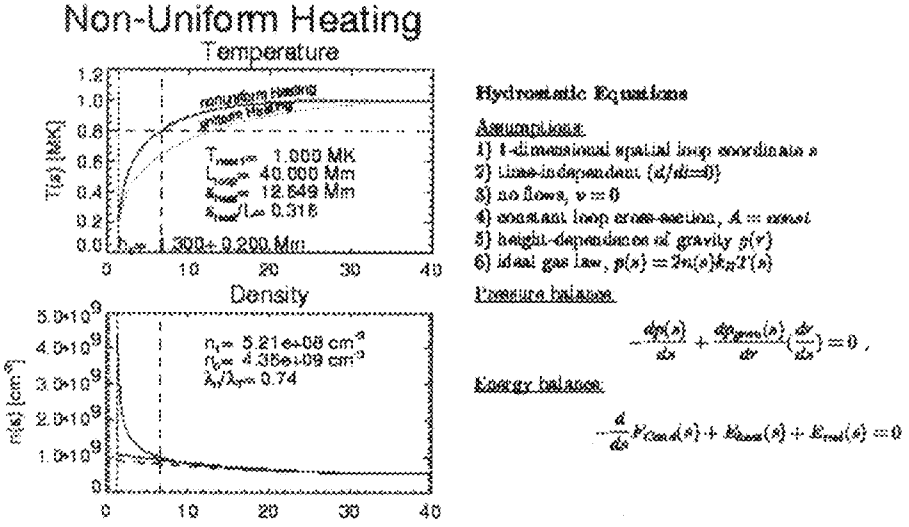

Hydrostatic Equations

Assumptions:
1) 1-dimensional spatial loop coordinate *s*
2) time-independent ($\partial/\partial t = 0$)
3) no flows, $v = 0$
4) constant loop cross-section, $A = const$
5) height-dependence of gravity $g(r)$
6) ideal gas law, $p(s) = 2n(s)k_B T(s)$

Pressure balance:

$$-\frac{dp(s)}{ds} + \frac{dg_{sun}(s)}{dr}\left(\frac{dr}{ds}\right) = 0 \,,$$

Energy balance:

$$-\frac{d}{ds}F_{cond}(s) + E_{heat}(s) + E_{rad}(s) = 0$$

A set of 3 physical parameters (n_e0=base density, E_H0=base heating rate, s_H=heating scale height) fully constrains a hydrostatic (steady-state) solution, T(s), n_e(s), and the emission measure EM(T[s])=n_e(T[s])^2

The steady-state solution is defined by the energy balance between the heating rate E_H(s), the radiative loss E_rad(s), and the conductive loss F_cond(s).

Recent analysis of TRACE data show that the heating scale height is confined to the footpoints, within a height range of s_H < 20,000 km (Aschwanden et al. 2000, ApJ 541, 1059).

Instrumental Response Function R(T)

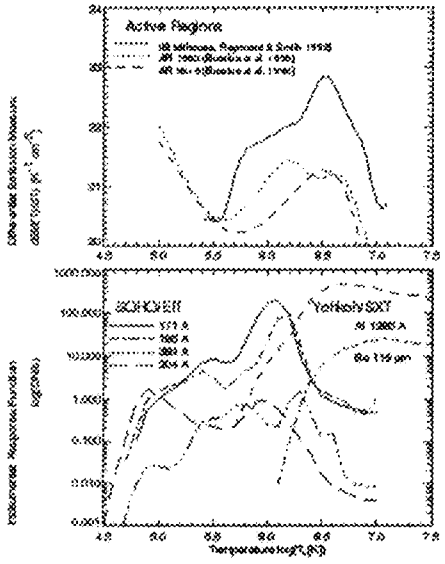

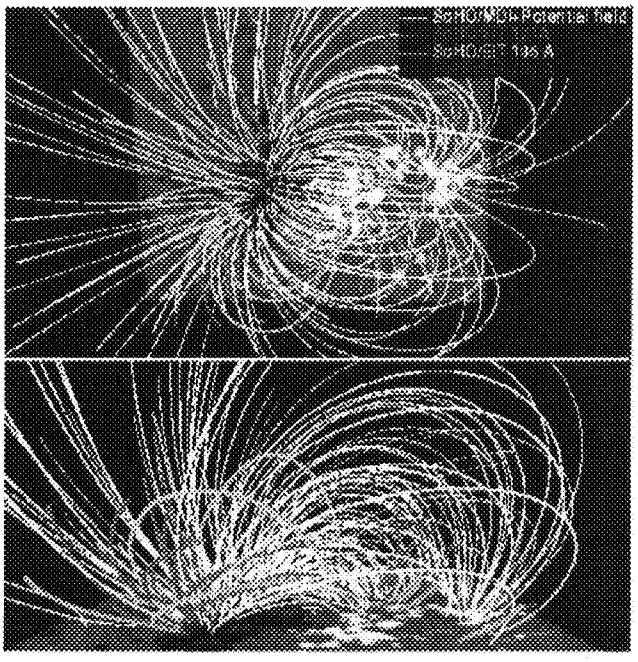

Physical model n_e(s), T(s) -> Differential emission measure distribution dEM(T[s])/dT,
Integration along line-of-sight z to obtain dEM(T)/dT.
Convolution with instrumental response functions R_171(T), R_195(T), R_211(T)
Intensity distribution I(x,y) in each passband 171, 195, 211 A
EIT and TRACE data show that EUV loops are near-isothermal and not co-spatial in different temperatures.

3D Model of Loop Arcades

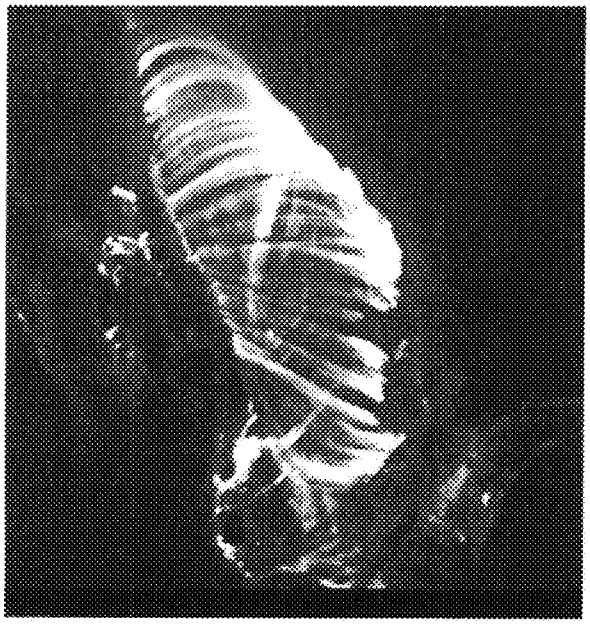

Observations :

TRACE 171 A observations of 1998 Sept 30, 14:30:05 UT. The image shows a post flare arcade, containing some 100 resolved loop threads with a separation of less than 1000 km each, indicating a heigh degree of fragmentation in the flare energy release region. The field of view has a size of 180,000 km, the image has 500x500 pixels.

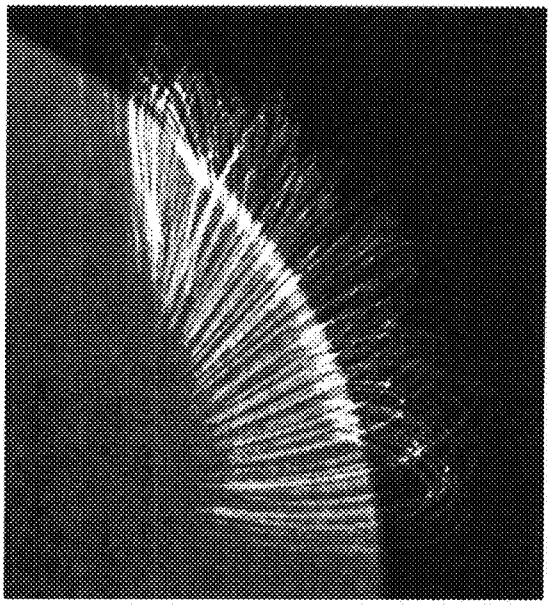

3D Model:

This 3D model contains 200 semi-circular loops, each one parametrized with 7 parameters: loop radius and thickness, position (heliograph. longitude and latitude), orientation (azimuth, inclination), and brightness. The image has 500x500 pixels.

Movie

STEREO/EUVI Science at LMSAL

1.Static 3D Reconstruction and Modeling

- Features: AR Loops, Quiescent filaments, prominences (TRACE obs.)
- Automated feature detection algorithm (Strous code)
- 3D-parametrization s(x,y) + variable z(x,y) --> s(x,y,z)
- Physical model, hydrostatic equations (n_e0, E_H0, s_H), dDEM/dT
- Instrumental response function ne(s),T(s)-->R(T)-->I_171(x,y)
- Stereoscopic tiepoints vs. Forward-fitting of 3D model

- Science quests:
  - Coronal heating function (E_H0, s_H)
  - Density scale heights, diagnostic of static vs. dynamic state
  - Magnetic field models (deviations from potential field)
  - Helicity, chirality, twist of filaments, sigmoids
  - Pre-eruptive physical conditions, sigmoids
  - Shear and twist threshold for kink instability or eruption
  - EUV Scattering in corona

Coronal Heating [n_e0, E_H0, s_H]

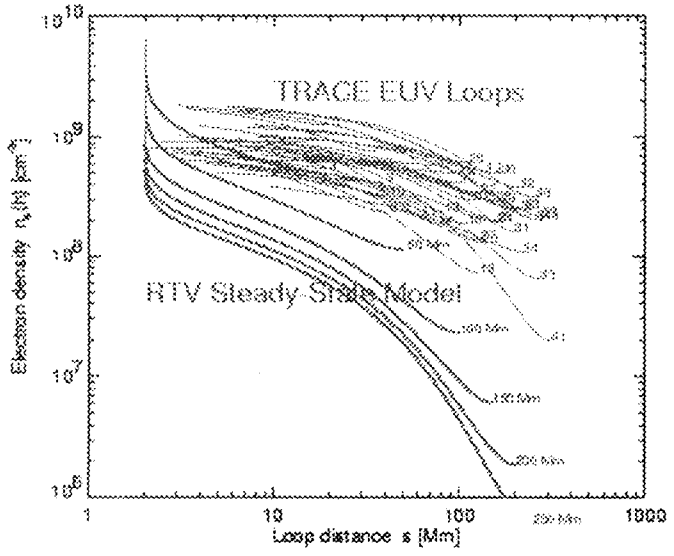

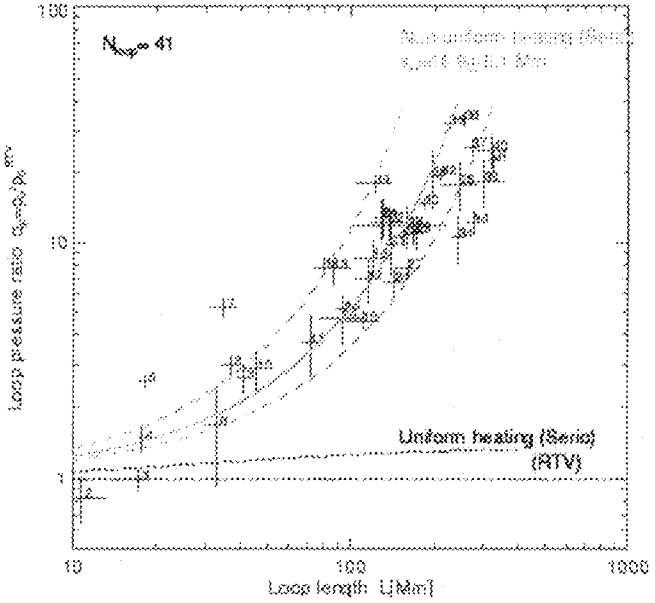

The heating rate (E_H0) and heating scale heights (s_H) of coronal loops can be determined for near steady-state loops from the energy balance with radiative and conductive losses.

Previous analysis of EUV loops have uncertainties in the electron density (background subtraction, loop width measurements, filling factor) and vertical density scale heights (loop inclination angle).

STEREO provides much better densities for loops (two independent background subtractions, two independent width measurements) and much better density scale heights (3D reconstruction of loop inclination angle).

Uniform vs. Nonuniform Heating

Uniform heating (Rosner-Tucker-Vaiana model) predicts a steeper temperature gradient, lower densities, and lower pressures than observed with EIT and TRACE. The uniform heating assumption is therefore not consistent with observations.

Non-uniform heating localized at the footpoints predicts near-isothermal (coronal) temperature profiles, higher pressures, and is consistent with EIT and TRACE measurements. The best-fit heating scale height is s_H=10-20 Mm for loops with half lenghts of L=10-300 Mm (Aschwanden et al. 2000, ApJ 541, 1059).

Density Scale Heights [s_L]

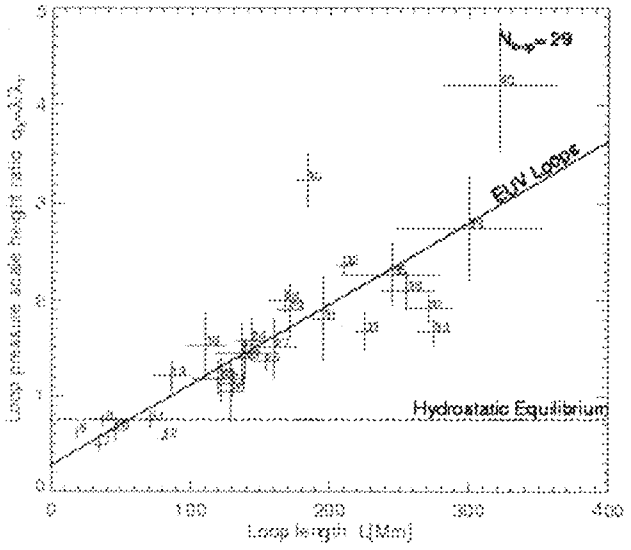

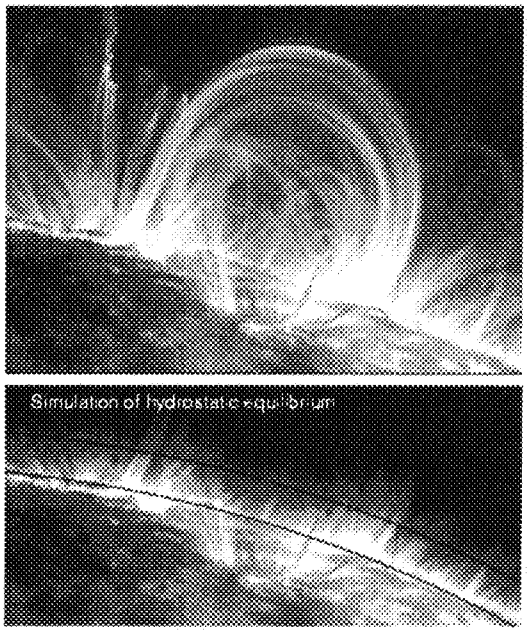

The density scale height (s_L) provides a diagnostic whether a loop is in hydrostatic (gravitational) equilibrium or in a dynamic state, boosted by overpressure from upflowing plasma or wave pressure.

Previous analysis of EUV loops have uncertainties in the electron density (background subtraction, loop width measurements, filling factor) and vertical density scale heights (loop inclination angle).

STEREO provides much better densities for loops (two independent background subtractions, two independent width measurements) and much better density scale heights (3D reconstruction of loop inclination angle).

Coronal Magnetic Field B(x,y,z)

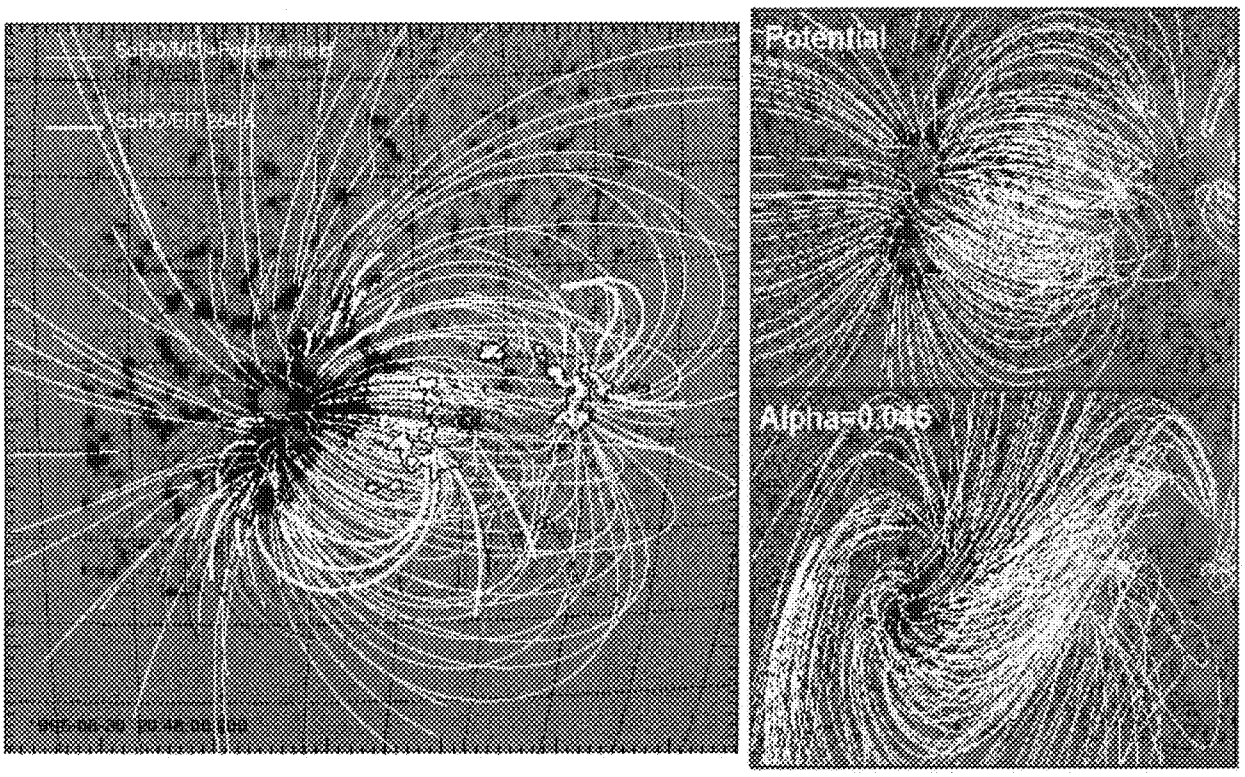

There are 2 independent methods to determine the coronal magnetic field: (1) by extrapolation from photoshperic magnetograms, using a theoretical model (potential, force-free, constant alpha, ...), and (2) by 3-dimensional stereoscopic reconstruction of magnetic field lines traced out by EUV-emitting plasma. Comparisons of the two methods provides the most accurate tests to-date of theoretical magnetic field models. A reliable diagnostic of non-potential fields provides invaluable information on coronal currents, shearing, twisting, magnetic energy build-up before flares and CMEs, estimate of released magnetic energy in flares and CMEs, detection of current sheets, separatrices, null points, energy comparison between closed-field and open-field state, etc.

Magnetic Chirality and Helicity B(VxB)

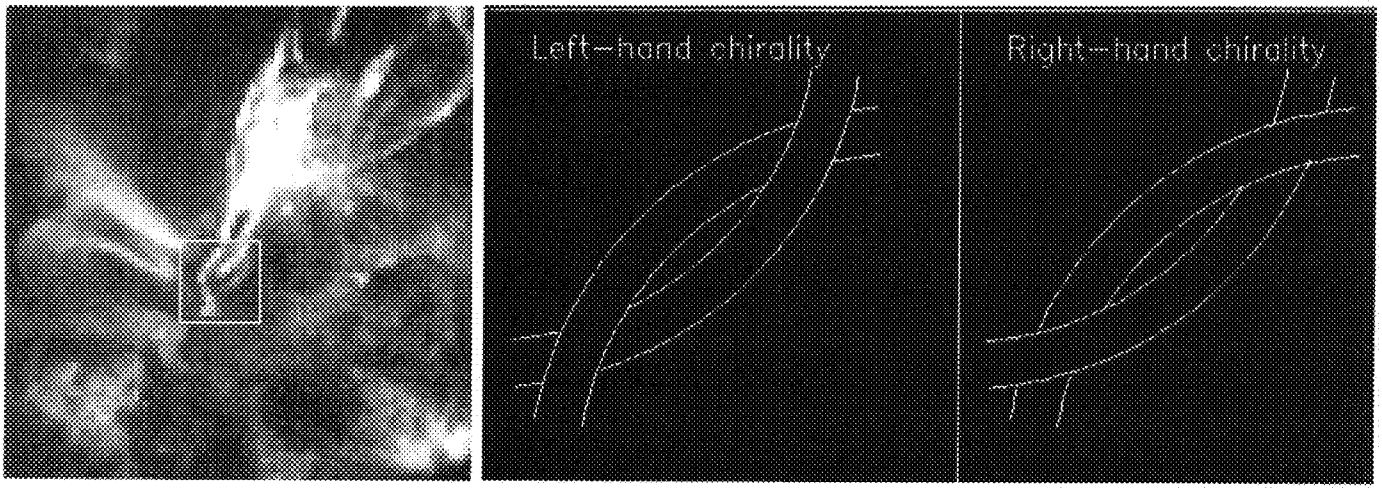

The chirality of the solar magnetic field is hemisphere dependent - the magnetic field in the northern/sourthern hemisphere has negative/positive helicity (Canfield, Pevtsov)

Dextral/sinistral filaments have negative/positive magnetic helicity, thus the hemisphere pattern of filament chirality is the same one as for active-region helicity (Chae 2000, ApJ 540, L115)

STEREO provides helicity measurements of magnetic arcades, filaments, prominences that produce CMEs, and allows for tests whether the helicity is conserved in erupting flux ropes and mangetic clouds.

Sigmoids and Eruptivity

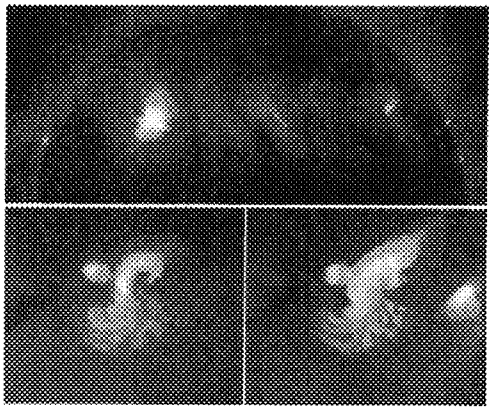

Yohkoh, SXT, 16-Jan-1993

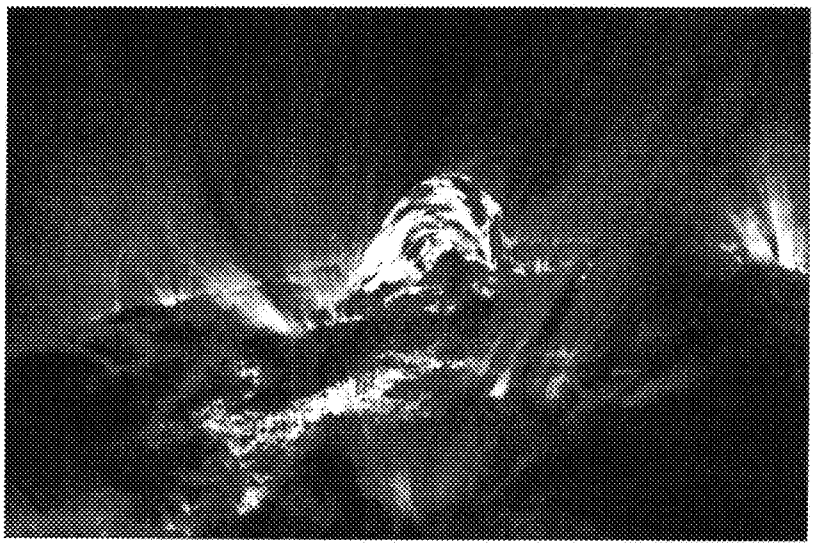

TRACE, 171 A, 29-Sept-2000

The sigmoid shape can be used as an indicator of the likelihood that an active region will erupt, and thus has some predictional capabilities of CME occurrence (Sterling and Hudson 1997, ApJ 491, L55; Hudson et al. 1998, GRL 25, 2481; Canfield, Hudson, and McKenzie 1999, GRL 26/6, 627).

STEREO can reveal the helical geometry of sigmoids in terms of 3D coordinates, can measure the helical twist angle, distinguish positive and negative helicity, and measure the critical twist angle before a kink instability or an eruption occurs.

STEREO/EUVI Science at LMSAL

2. Dynamic 3D Reconstruction and Modeling

- Features: Dynamic, flaring, post-flare loops, eruptive filaments & prominences, CMEs, EIT/Moreton waves, coronal dimming
- Basic steps are similar to static 3D-reconstruction of stereo image pairs
- Additional constraints: trajectories s(,x,y,z,t) -> v(t)=ds/dt, a(t)=dv/dt
- Hydrodynamic equations with velocity-related terms v(s,t)
- Coordinate transformation for expanding systems, s(t) -> s'(t)

- Science quests:
  - Coronal heating: Time variability and intermittency of heating function E_H0(t), s_H(t)
  - Catastrophic cooling: coroanl loops become unstable for short heating scale heights
  - Mass flow diagnostics: siphon flows in loops, chromospheric upflows
  - Magnetic reconnection: 3D topology, 2D current sheets, spines, fans, null points
  - CME trigger: evolution of heating and cooling in eruptive phenomena, flares, CMEs
  - Magnetic instability: onset of instabilities as function of change in shear, twist, heating rate
  - Dynamics of eruptive phenomena: speed, acceleration, forces (E + vxB)
  - Waves: 3D propagation characteristics of EIT/Moreton waves
  - EUV Dimming: first accurate maeasurements of 3D volume and mass of evacuated material

Dynamic parametrization of 3D geometry s(x,y,z,t)

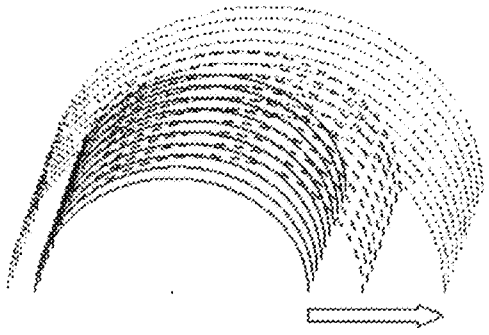

Dynamic coordinates of loop arcade

The coordinates of linear one-dimensional features (e.g. loops, filaments) are parameterized with a length coordinate s(x,y,z,t) as function of 3D cartesian coordinates (x,y,z) and time t in an inertial frame anchored on the solar surface.

Heliographic longitude : l(t) = l_0 + (dl/dt) (t-t_0) + ... --> motion
Heliographic latitude : b(t) = b_0 + (db/dt) (t-t_0) + ... --> motion
Heliographic altitude : h(t) = h_0 + (dh/dt) (t-t_0) + ... --> rise, expansion
Azimuth angle : A(t) = A_0 + (dA/dt) (t-t_0) + ... --> rotation, twisting
Inclination angle : I(t) = I_0 + (dI/dt) (t-t_0) + ... --> tilting

Physical model from hydrodynamic equations

HYDRODYNAMIC EQUATIONS

Mass Conservation,

$$\frac{\partial n}{\partial t} + \frac{1}{A}\frac{\partial}{\partial s}(nvA) = 0$$

Momentum equation,

$$mn\frac{\partial v}{\partial t} + mnv\frac{\partial v}{\partial s} = -\frac{\partial p}{\partial s} + \frac{\partial p_{grav}}{\partial s}(\frac{1}{A})$$

Energy equation (in conservative form),

$$\frac{1}{A}\frac{\partial}{\partial s}(nvA[\epsilon_{enth} + \epsilon_{kin} + \epsilon_{grav}] + AF_{cond}) = E_{heat} + E_{rad}$$

Total pressure $p(s)$ of a fully ionized gas

$$p(s) = [n_e(s) + n_i(s)]k_B T(s) = 2n(s)k_B T(s$$

Enthalpy energy $\epsilon_{enth}(s)$:

$$\epsilon_{enth}(s) = \frac{5}{2}k_B T(s) ,$$

Kinetic energy $\epsilon_{kin}(s)$:

$$\epsilon_{kin}(s) = \frac{1}{2}mv^2(s) ,$$

Gravitational potential $\epsilon_{grav}(s)$:

$$\epsilon_{grav}(r) = \frac{GM_\odot m}{r} = mg_\odot(\frac{R_\odot^2}{r}) ,$$

solar gravitation $g_\odot = GM_\odot/R_\odot^2 = 2.74 \times 10^4$ cm s^{-2} Gravitati

$$\frac{d\epsilon_{grav}}{ds}(r) = -mg_\odot(\frac{R_\odot^2}{r^2}) .$$

Generalization : hydrostatic --> hydrodynamic model

Mass flows in linear structures: v(s)

Flux tube expansion or width variation: A(s)

Time-dependent evolution: n_e(s,t), p(s,t), T(s,t), v(s,t), A(s,t)

Coordinate transformation for expanding systems: s(t) -> s'(t)

Dynamic 3D Reconstruction and Modeling : Science

- Coronal heating: Time-dependent loop modeling reveals time variability and intermittency of heating function E_H0(t), s_H(t)
- Catastrophic cooling: when heating scale height (s_H) decreases, steady-state solution yields density inversion, whereafter loops become unstable
- Mass flow diagnostics: 3D reconstruction of mass flows yields true velocity (not only projected velocity), -> diagnostic of subsonic, supersonic flows
- Evolution of eruptive phenomena: filaments, flares, CMEs
  Dynamics of eruptive phenomena: speed, acceleration, forces (E + vxB)
- Magnetic reconnection: disentangling of 3D topology, 2D current sheets, spines, fans, null points, before and after reconnection
- Onset of magnetic instabilities as function of change in shear, twist, heating rate
- Waves: 3D propagation characteristics of EIT/Moreton waves
- EUV Dimming: first accurate maeasurements of 3D volume and mass of evacuated material

STEREO/EUVI Science at LMSAL

Technical and Methodical Issues

1. Spatial resolution, ISS (threads, filling factor, contrast, chirality, crossings, altitude fading)
2. Aspect angle separation vs. optimum science (parallax versus confusion)
3. Physical modeling (forward-fitting vs. inversion)
4. EUVI software approach of LMSAL group

Spatial Resolution : Number Limit of Resolved Structures

For a number of STEREO experiments, the number of detected (resolved) fine structures in the solar corona represents a principal limit for specific scientific questions, for instance:

1. What is a coronal loop made off? Of how many loop threads? (This is important for any type of temperature and density models, because each thread has a different maximum temperature, and is likely to have a different heating function.)
2. What is the filling factor of a coronal loop?
3. What is the true electron density of a loop? (depends on filling factor)
4. What is the geometric size of elementary heating processes ? (related to cross-sections of smallest loop threads)

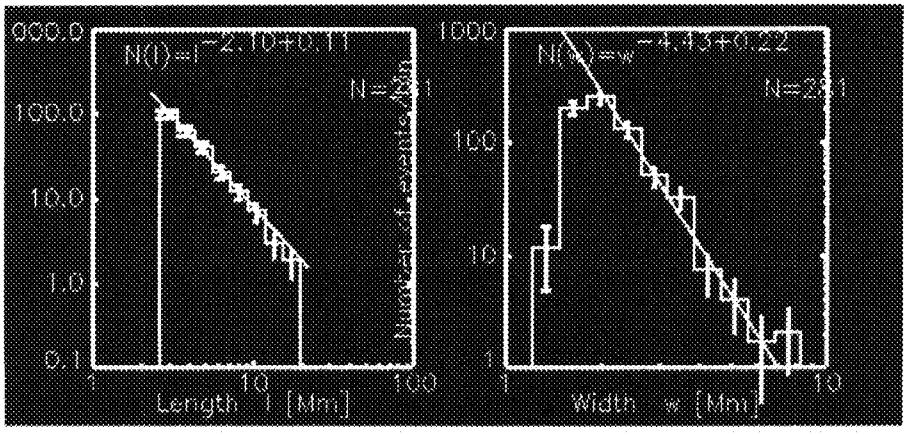

Fig.1: Distribution of loop lengths and widths. There is not much systematic statistics on loop fine structure in the literature. As a quantitative example we use the statistics of 281 nanoflare loops, detected with TRACE at 171 A (Aschwanden et al. 2000, ApJ 535:1047, Fig.4), using an automated algorithm and 4x4 macropixels, which produces a cutoff of 2"≈1.4 Mm for spatial scales. The histograms above show the distributions of loop lengths and loop widths, which are found to have a power-law distribution with slopes of -2 (for loop lengths) and -4 (for loop widths). A decrease in resolution by a factor of 2.5 would therefore provide a decrease in detected loop fine structure by a factor of 2.5^4=40.

Spatial Resolution : Threads of Loops and Filaments

1. Does an apparent sigmoid structure (leading to a CME) consist of unsheared (straight) segments, or strongly-sheared S-segments ?
2. What is the true shear of filament threads ? (threads can be arbitrarily more sheared than the rope shape)
3. Does an erupting (or quiescent) flux rope consist of helical threads and what is the critical twist angle before it erupts? (Important for diagnostic of kink-instability as CME trigger)
4. What is the magnetic topology at the location of a filament eruption (leading to a CME)? What type of magnetic reconnection (I-, X-, Y-type) triggers the eruption? (The determination of the topology requires resolving the finest details in the reconnection region).

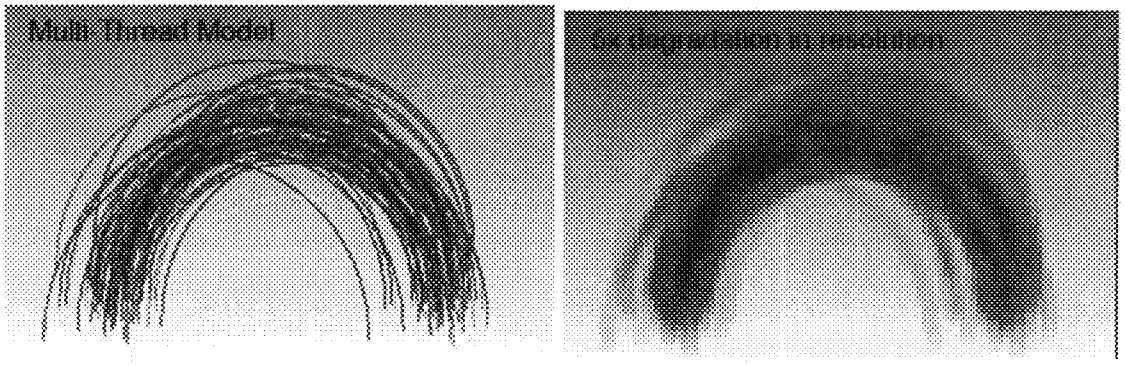

Fig.2: Insufficient resolution of loop threads is visualized in this simulation, showing 100 loop threads, rebinned to 5 times degraded resolution. Note that the degraded instrument allows to resolve about 5-10 strands from this bundle of 100 threads. The reduced number of discerned structures does not scale linearly, but rather with the 2nd power (for parallel features) to the 3rd power (i.e. with the volume density for truly three-dimensional features). In this example, a factor 5 loss in resolution allows to discern about 100^(1/2)=10 parallel features or about 100^(1/3)=5 truly three-dimensional features. The example of a bundle with twisted threads represents an intermediate case, so one expects to discern in the range of 5-10 threads. [Adapted from Fig.1 in Aschwanden et al. 2000 (Oct 1), ApJ 541:1059].

Contrast : Limit in Determination of Magnetic Topology

Another scientific question is the determination of the magnetic topology of erupting filaments, which bears an important information for understanding the magnetic evolution of CME flux ropes and magnetic clouds.

1. What is the orientation, helicity, and chirality of helical loop threads? (which requires to resolve the front end from the back end of helical segments along a line-of-sight)

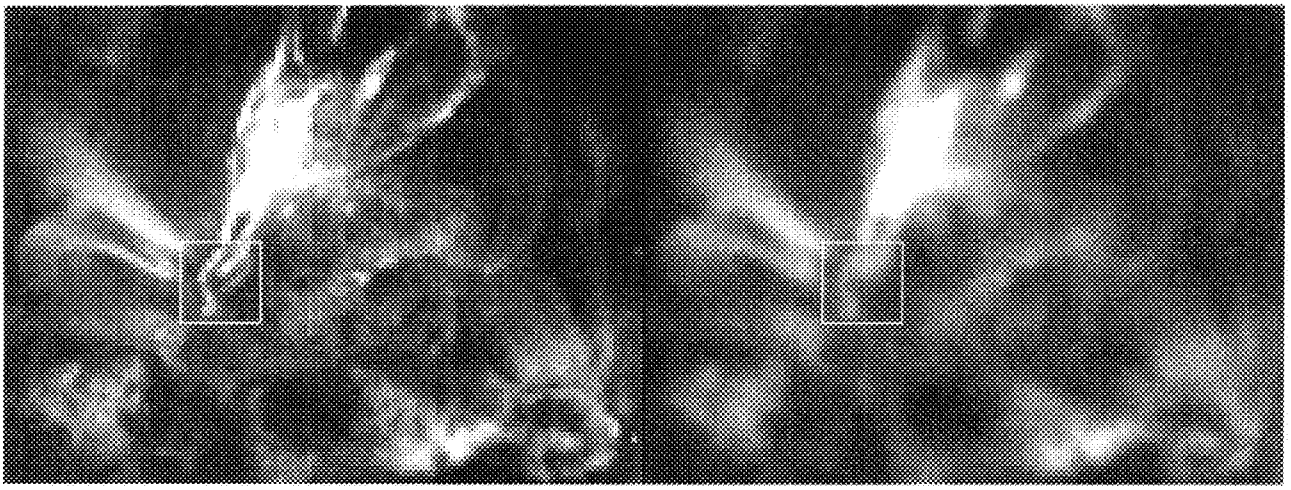

Fig.3: TRACE image of an eruptive filament, reduced to EUVI resolution with ISS (left frame) and without ISS (right frame), see movie on (http://www.lmsal.com/~wuelser/iss_descope.html). The square box encompasses a detail at the location where the filament eruption originated. The fine structure at the site of origin can clearly be recognized with ISS (left), consisting of 3 helical strands, while the same information cannot be retrieved from the image without ISS (right).

Contrast : Limit in Determination of Helicity

How do filament threads with sinistral or dextral chirality relate to positive and negative helicity ? (This question requires to resolve the front end from the back end of helical segments along a line-of-sight, see Chae 2000, ApJ 540, L115)

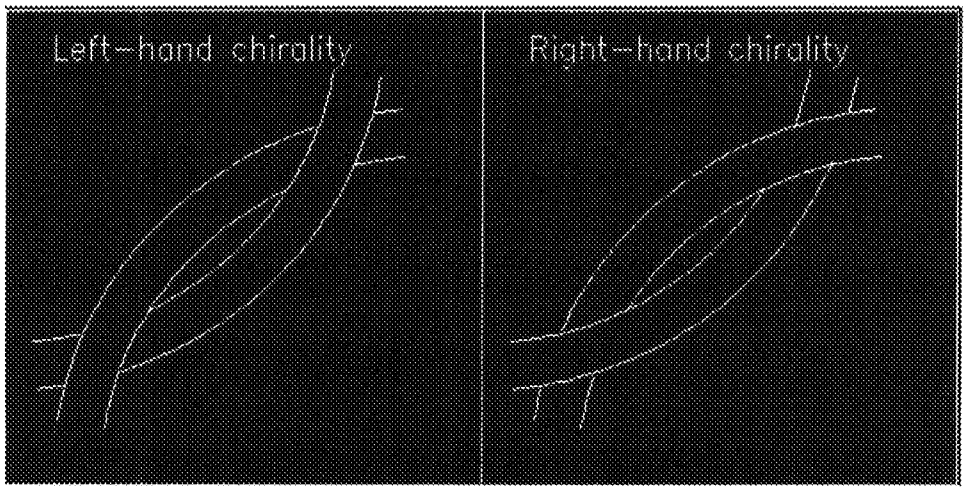

Fig.4: To determine the magnetic helicity sign of a filament one has to determine the dextral or sinistral chirality depending on its axial field direction. The magnetic helicity sign of a filament can be determined, if the two overlapping segments have non-equal brightness, e.g. a bright thread over a dark thread segment, or vice versa. Such a measurement has recently been demonstrated by Jongchul Chae (ApJ 540:L115, 2000 Sept 10), with the finding that the dextral filaments have negative magnetic helicity. This information is important to understand in what sense the twisting of filaments builds up sufficiently high shear for eruption or kink instability, which could explain the physical trigger mechanisms of CMEs. The observational determination of the chirality depends mainly on the relative brightness contrast of the two overlapping segments. If we set a 3-sigma threshold for a minimum contrast, the critical limit is proportional to the square root of the photon statistics, i.e. 3 sigma = 3*sqrt(N). For a degraded resolution by a factor of 2.5, two overlapping structures have a cross-section enlarged by a factor of 2.5, and thus a factor of 2.5^2=6 higher photon statistics is required to warrant the same critical contrast. Therefore, the magnetic chirality can only be determined for 6 times brighter filaments without ISS.

Magnetic Helicity Sign of Filament Chirality

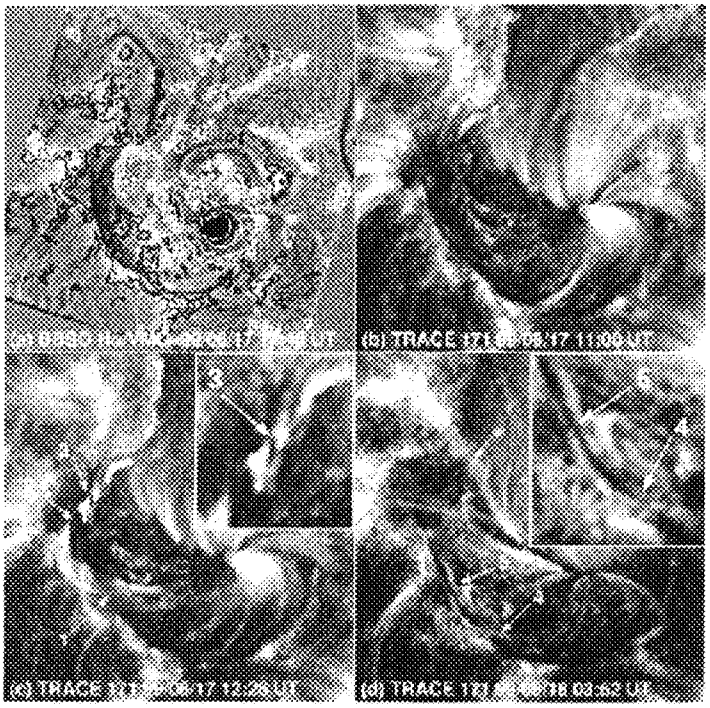

Observed thread crossings in an inverse S-shaped filament. Note that the filament is dextral. (a) High-resolution H-alpha data and line-of-sight magnetogram taken at BBSO. The positive flux density levels are represented by white contours, and the negative ones by black contours. (b-d) TRACE images at different times. The helicity is mearured at crossing points of overlying dark threads over underlying bright threads, or vice versa (from Fig.2 in Chae 2000, ApJ 540, L115).

Contrast : Scale-Height Limit in Tracing Loops or Filaments in Altitude

Many coronal structures have a density distribution close to hydrostatic equilibrium, although strong deviations are likely during dynamic phases (flares, filaments, etc.) This means that the density drops about a factor e^2=10 over 2 scale heights, and the emission measure (proportional to squared density) drops a factor of e^4=100. Practically, that means that the upper parts of loops above 2 scale heights (for a detection threshold of 1%) are undetectable. This is particularly troublesome for eruptive phenomena, which we want to trace far out into the upper corona to understand the evolution of eruptive filaments in the context of the CME evolution. If the resolution is degraded by a factor of 2.5 (without ISS), the photons of a linear structure are smeared out over a cross-section enlarged by a factor of 2.5. This produces a 2.5 lower number of photons per pixel at the peak of the structure, and a proportionally smaller contrast between adjacent pixels. Using a 3-sigma criterion for a detection threshold, which scales with the square root of the photons per pixel, the structure has to be 2.5^2=6 times brighter to warrant the same contrast. For hydrostatic loops, this means that they will fade out and become undetectable at a lower altitude. For instance, at 171 A (T=1 MK, scale height L=50 Mm), with a detection threshold of 1%, loops or filaments can be traced up to a height of 2.3 scale heights, i.e. 115 Mm, because EM/EM_0=[exp(-2.3)]^2=0.01 with ISS. Without ISS, the contrast needs to be 6 times higher, which allows only tracing up to an altitude of 1.4 scale heights, i.e. 70 Mm, because EM/EM_0=[exp(-1.4)]^2=0.06.

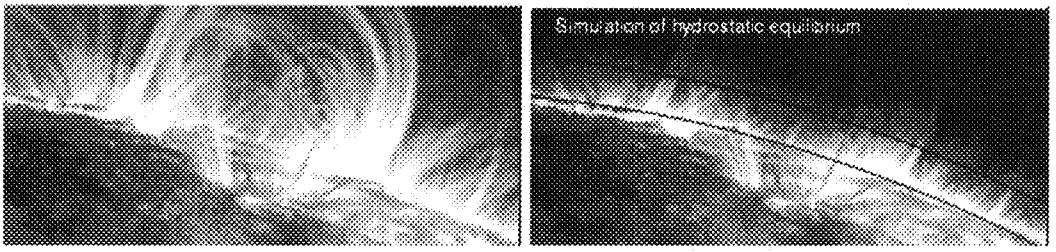

Fig.5: TRACE image of coronal loops observed in 171 A on 1999 Nov 6, 02:22 UT. The upper part shows the observed data, which have obviously super-hydrostatic scale heights, otherwise the looptops would not be visible. Such visibility in excess of about two hydrostatic scale height may only be available during the most dynamic phases of a filament eruption or postflare phase. - The bottom part shows a simulated image of the same data scaled to hydrostatic scale height (L=50 Mm in density, or L/2=25 Mm in emission measure, see altitude level indicated with black line). This situation is more typical for quiescent corona, or after gravitational settlement of an eruption. This comparison demonstrates the drastic altitude limitation of detectability for hydrostatic structures.

Importance of Image Stabilization System (ISS) for STEREO science

The EUVI imager has a basic angular resolution defined in terms of a pixel size of 1.6" (i.e.1.0 Mm). Descoping of the Image Stabilization System (ISS) would produce a degradation of the image resolution by an approximate factor of 2.5. Here we investigate in a quantitative manner what the consequences of such a reduction in image resolution would be on scientific data analysis.

Conclusions

1. The number of resolved loop threads, which is an important limit to infer correct physical parameters and magnetic topology, scales with about the third power (i.e. volumetric density) of the linear resolution. A degradation by a factor of 2.5 (without ISS) would reduce the number of resolved loop threads by about 2.5^3=16.

2. Insufficient resolution of individual loop threads, which are supposedly thermally separated, implies averaging over different temperature profiles, different density scale heights, and different heating functions. The determination of any coronal heating function from such averaged structures is thus ambiguous and the time average may not be representative for the true (time-dependent) heating function.

3. A degradation of the resolution by a factor of 2.5 requires 6 times brighter structures to show the same contrast between overlapping foreground and background structures. This has severe consequences to disentangle the magnetic morphology of structures overlapping along the line-of-sight, e.g. for the determination of the magnetic chirality or to relate the stereoscopic tiepoints of corresponding structures in 2 stereo images.

4. The tracing of structures such as loop threads or filaments is drastically limited in altitude due to the exponentailly falling-off density with height. For a detection threshold of 1% of the footpoint brightness, hydrostatic loops can approximately be traced up to 2.3 scale heights. For reduced image resolution by a factor of 2.5 (without ISS), the same structures can only be traced up to heights of 1.4 scale heights with the same contrast.

Descoping the Image Stabilization System (ISS) ?

In conclusion, a reduction of the image resolution, as it would be caused without ISS, would severly restrict spatial resolution, contrast, detectability, and the ability to disentangle fine structures. The disentangling of fine structure is especially important because stereoscopic correlation can only be accomplished if the TRULY CORRESPONDING structures are combined, while ERRONEOUS COMBINATIONS of stereoscopic tiepoints lead to completely meaningless stereoscopic results. It is therefore highly recommendable to operate both STEREO spacecraft with ISS, in order to achieve correct stereoscopic correlations and many science goals that rely on a sensible disentangling of fine structures (e.g. loop threads, filament threads, helicity and chirality of flux ropes, magnetic topology in magnetic reconnection regions.)

Web documents on technical aspects of SECCHI/EUVI/ISS see :
http://www.lmsal.com/~wuelser/iss_descope.html
http://www.lmsal.com/~wuelser/req.html
See also poster by Aschwanden & Wuelser (SECCHI Consortium Meeting)

Spacecraft Stereo-Angle Separation vs. Science

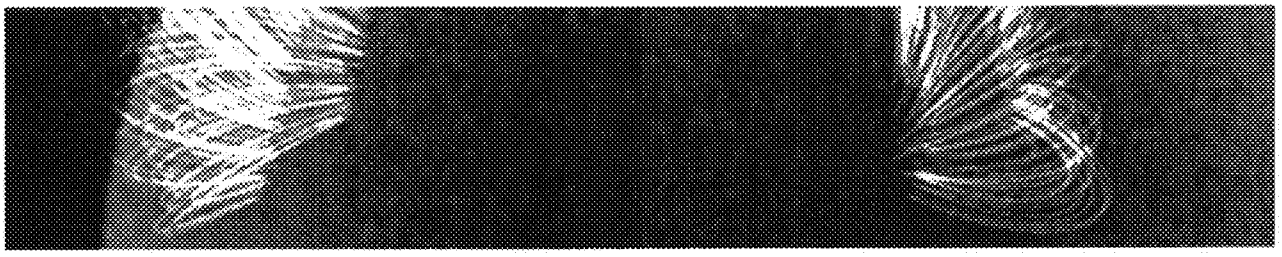

Small stereo angles (1-30 deg) are favorable for 3D reconstruction of linear structures (loops, filaments, flux ropes) because tiepoint identification has minimal confusion for small angles.

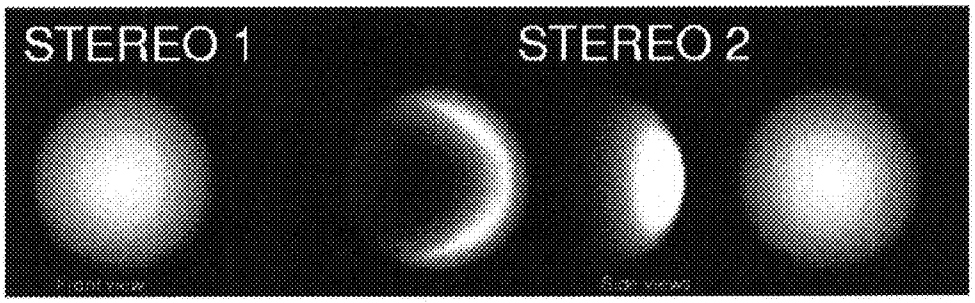

Large stereo angles (30-90 deg) are favorable for 3D reconstruction of voluminous structures (CME shell, magnetic cloud), because the surface topology is indistinguishable for small stereo angles, but optimum for orthogonal views.

SECCHI/EUVI Software Approach at LMSAL

- Physics drives numeric algorithms, concept, and design of software development
- Static (3D) and Dynamic (4D) Reconstruction Methods
- Use heritage of SolarSoftWare (SSW) used by Yohkoh, SoHO, TRACE, HESSI, and others. (FITS format already extended for spacecraft position by Bill Thompson)
  (CCD image processing routines exist: despiker, destreaker, moviemaker, etc.)
- Modular software package in IDL, perhaps object-oriented (overhead problem), running in unix and windows environments
- Tie in closely with software developments at JPL (visualization), NRL (CME codes), SAIC (MHD codes)

3D Models - Stereoscopy - Tomography

Search keywords: [3D] - Excl: []

Updated : 2000 Nov 14 06:52 - Number of entries: 119

2001

Aschwanden,M.J. and Acton,L.W.2001, ApJ, ... (revised, Aug 28, 2000)
Temperature tomography of the soft X-ray corona: measurements of electron densities, temperatures, and differential emission measure distributions above the limb

2000

Aschwanden,M.J., Alexander,D., Hurlburt,N., Newmark,J.S., Neupert,W.M., Klimchuk,J.A., and G.A.Gary2000, ApJ 531, 1129-1149,
3D-Stereoscopic Analysis of Solar Active Region Loops: II. SOHO/EIT Observations at Temperatrures of 1.5-2.5 MK

Aschwanden,M.J., Wuelser,J.P.2000, STEREO/SECCHI/EUVI study, WWW document (Oct 2000)
STEREO/SECCHI/EUVI - Importance of Image Stabililzation System (ISS) for STEREO science

Aschwanden,M.J., Wuelser,J.P., Alexander,D., Metcalf,T., Nitta,N., Lemen,J., Wolfson,J., Hurlburt,N., R.Nightingale2000, STEREO/SECCHI Consortium Meeting, 2000 Nov 6-9, Easton, Maryland, WWW document
STEREO/EUVI Science at LMSAL

Birn,J., Gosling,J.T., Hesse,M., Forbes,T.G., Priest,E.R.2000, ApJ 541, 1078-1095
Simulations of three-dimensional reconnection in the solar corona

Craig,I.J.D. and Watson,P.G.2000, SP 194, 251-268,
Optimized magnetic reconnection solutions in three dimensions

Fletcher,L., Metcalf,T.R., Alexander,D., Ryder,L.A., and Brown,D.S.2000, ApJ ...
Evidence for the flare trigger site and 3-D reconnection in multi- wavelength observations of a solar flare

Forbes,T.G.2000, Adv.Spaced Res. 26/3, 549-556
Reconnection theory in three dimensions

Frazin,R.A.2000, ApJ 530, 1026-1035,
Tomography of the solar corona I. A robust, regularized, positive estimation method

Gibson,S.E. and Low,B.C.2000, ...
3D and twisted: an MHD interpretation of on-disk observational charateristics of CMEs

Grebinskij,A., Bogod,V., Gelfreikh,G., Urpo,S., Pohjolainen,S. and Shibasaki,K.2000, AASS, 144, 169,
Microwave tomography of solar magnetic fields

Petrie,G.J.D. and Neukirch,T.2000, AA 356, 735,
The Green's function method for a special class of linear three-dimensional magnetohydrostatic equilibria

Vedenov,A.A., Koutvitsky,V.A., Koutchmy,S., Molodensky,M.M. and Oraevsky,V.N.2000, Astronomy Report Vol. 44, No.2, pp.112-121,
On stereoimages of some structures in the solar atmosphere

1999

Aschwanden,M.J., Kosugi,T., Hanaoka,Y., Nishio,M., and Melrose,D.B.1999, ApJ 526, 1026-1045
Quadrupolar Magnetic Reconnection in Solar Flares: I.3D Geometry inferred from Yohkoh Observations

Aschwanden,M.J., Newmark,J.S., Delaboudiniere,J.P., Neupert,W.M., Klimchuk,J.A., Gary,G.A., Portier-Fornazzi,F., and Zucker,A.1999, ApJ 515, 842-867
Three-dimensional stereoscopic analysis of solar active region loops: I. SOHO/EIT observations at temperatrures of 1.0-1.5 MK

Aulanier,G., Demoulin,P., Mein,N., VanDriel-Gesztelyi,L., Mein,P., and Schmieder,P.1999, AA 342, 867-880,
3-D magnetic configurations supporting prominences. III. evolution of fine structures observed in a filament channel

Demoulin,P., Aulanier,G., and Schmieder,B.1999, in B. Schmieder, A. Hofmann, J. Staude (eds.), 'Third Advances in Solar Physics Euroconference: Magnetic Fields and Oscillations', ASP Conference Series 184, 65-69,
Some advances in 3D-magnetic field topology: an observed case of a "bald patch" flare

Dorch,S.B.F., Archontis,V. and Nordlund,A.1999, AA, 352, L79
3D simulations of twisted magnetic flux ropes

Filippov,B.P.1999, SP 185, 297-309,
Observation of a 3D magnetic null point in the solar corona

Gary,A. and Alexander,D.1999, SP 186, 123-139,
Constructing the coronal magnetic field by correlating parametrized fieldlines with observed coronal plasma structures

Hudson,H.S. and Wheatland,M.S.1999, SP 186, 301-310
Topological differences between force-free field models

Kondrashov,D., Feynman,J., Liewer,P.C., and Ruzmaikin,A.1999, ApJ 519, 884-898,
Three-dimensional (3-D) magnetohydrodynamic simulations of the interaction of magnetic

flux tubes

Koutchmy,S., Matsuura,O., Molodensky,M.M., Picazzio,E., and Starkova,L.I.1999, Astronomy Reports, Vol. 43, No.3,
The plane of polarization of the solar corona during eclipse observations

Koutchmy,S., Molodensky,M.M., Matsuura,O.T., and Picazzio,E.1999, Astronomy Letters, Vol. 25, No.4, pp.258-262,
Steady-state configuration of the heliospheric sheet

Kucera,T.A., Aulanier,G., Schmieder,B., Mein,N., Vial,J.C.1999, SP 186, 259-280
Filament channel structures in a Si IV line related to a 3D magnetic model

Morita,S., Uchida,Y., Hirose,S., Uemura,S., and Yamaguchi,T.1999, in "Solar Physics with Radio Observations", Nobeyama Radio Observatory NRO Report No. 479, Proc. of Nobeyama Symp. 1998, (eds. T.Bastian, N.Gopalswamy, and K.Shibasaki), p.413-417,
Derivation of the 3D structure of flares in the homologous flare series of 1992 February

Nitta,N., VanDriel-Gestelyi,L., and Harra-Murnion,L,K.1999, SP 189, 181-198.
Flare loop geometry

Odstrcil,D. and Pizzo,V.J.1999, JGR, 104, 228225,
Distortion of the interplanetary magnetic field by three-dimensional propagation of coronal mass ejections in a structured solar wind

VanAalst,M.K., Martens,P.C.H. and Belien,A.J.C.1999, ApJL 511, L125,
Can streamer blobs prevent the buildup of the interplanetary magnetic field?

Zidowitz,S.1999, JGR 104/A5, 9727-9734,
Coronal structure of the whole sun month: a tomographic reconstruction

1998

Alexander,D., Gary,G.A., Thompson,B.J.1998, in 2nd Advances in Solar Physics Euroconverence, Three-dimensional Structure of Solar Active Regions, Astron.Soc.Pac. Conf.Ser. 155, (eds. C.E.Alissandrakis and Schmieder,B.), p.100-104,
Analysis of active regions via 3D rendering techniques

Aschwanden,M.J., Bastian,T.S., Nitta,N., Newmark,J., Thompson,B.J. and Harrison,R.A.1998, in Proc. 2nd Advances in Solar Physics Euroconference, "Three-Dimensional Structure of Solar Active Regions, held in Preveza, Greece, 1997 Oct 7-11, (eds. C.Alissandrakis and B.Schmieder) PASP 155, 311-315
Coordinated Observations with SOHO, Yohkoh, and VLA

Aschwanden,M.J., Neupert,W.N., Newmark,J., Thompson,B.J., Brosius,J.W., Holman,G.D., Harrison,R.A., Bastian,T.S., Nitta,N., Hudson,H.S., and Zucker,A.1998, in Proc. 2nd Advances in Solar Physics Euroconference, "Three-Dimensional Structure of Solar Active Regions, held in Preveza, Greece, 1997 Oct 7-11, (eds. C.Alissandrakis and B.Schmieder) PASP 155, 145-149
3-Dimensional Models of Active Region Loops

Aulanier,G. and Demoulin,P.1998, AA 329, 1125,
3-D magnetic configurations supporting prominences. I. The natural presence of lateral feet

Aulanier,G., Demoulin,P., VanDriel-Geztelyi,L., Mein,P., DeForest,C.1998, AA 335, 309,
3-D magnetic configurations supporting prominences. II. The lateral feet as a perturbation of a twisted flux-tube

Aulanier,G., Schmieder,B., Demoulin,P., vanDriel-Gesztelyi,L., and DeForest,C.1998, in 2nd Advances in Solar Physics Euroconverence, Three-dimensional Structure of Solar Active Regions, Astron.Soc.Pac. Conf.Ser. 155, (eds. C.E.Alissandrakis and Schmieder,B.), p.105-109,
Nonpotentiality of coronal loops above active regions

Gary,A., Davis,J.M., and Moore,R.1998, SP 183, 45-76,
On analysis of dual spacecraft stereoscopic observations to determine the three-dimensional mosphology and plasma properties of solar coronal flux tubes

Gelfreikh,G.B.1998, in 2nd Advances in Solar Physics Euroconverence, Three-dimensional Structure of Solar Active Regions, Astron.Soc.Pac. Conf.Ser. 155, (eds. C.E.Alissandrakis and Schmieder,B.), p.110-129,
Three-dimensional structure of the magnetosphere of solar active regions from radio observations

Kane,S.R., Hurley,K., McTiernan,J.M., Boer,M., Niel,M., Kosugi,T. and Yoshimori,M.1998, ApJ 500, 1003-1008,
Stereoscopic observations of solar hard X-ray flares made by Ulysses and Yohkoh

Somov,B.V., Kosugi,T. and Sakao,T.1998, ApJ 497, 943-956
Collisionless 3D reconnection in impulsive solar flares

1997

Antiochos,S.K.1997, SP 174, 5-19,
The implications of 3D for solar MHD modeling

Bogod,V.M., and Grebinskij,A.S.1997, SP 176, 67-86
Large-scale structure of atmosphere of the quiet sun, coronal hole, and plages as deduced by tomography study

Crooker,N., Joselyn,J.A., and Feynman,J. (eds.)1997, Geophys.Monogr.Ser. Vol.99, AGU Washington DC,
Coronal mass ejections

Gary,A.1997, SP 174, 241-263,
Rendering three-dimensional solar coronal structures

Koutchmy,S., Molodensky,M., and Vibert,D.1997, in IAU Symp 167, Proc. ASP 150, (D.Webb et al.), "New Perspectives on Solar Prominence", p.127,
A model of plasma sheets in equilibrium

Koutchmy,S., Molodenskii,M.M., Starkova,L.I., Kutvitskii,V.A., and Ershov,A.V.1997, Astronomy Letters, Vol. 23, No.6, pp. 818-826,
The heliospheric layer and the coronal structure on November 3, 1994

Lites,B.W., and Low,B.C.1997, SP 174, 91-98,
Flux emergence and prominences: a new scenario for 3-dimensional field geometry based on observations with the advanced Stokes polarimeter

McClymont,A.N., Jiao,L., and Mikic,Z.1997, SP 1997, SP 174, 191-218,
Problems and progress in computing three-dimensional coronal active region magnetic fields from boundary data

Moore,R.L., Schmieder,B., Hathaway,D.H., and Tarbell,T.D.1997, SP 176, 153-169,
3D Magnetic field configuration late in a large two-ribbon flare

Rust,D.M. et al. (eds.)1997, Report of the NASA Science Definition Team for the STEREO Mission,
The sun and heliosphere in three dimensions

Schmieder,B., Demoulin,P., Malherbe,J.M., Roudier,T., Nitta,N., and Harra-Murnion,L.K.1997, Adv.Space Res. 18/12, 1871
3D reconnection related to new emerging flux

Zidowitz,S.1997, in 5th SOHO Workshop on "The Corona and Solar Wind near Minimum Activity", ESA SP-404, p.757-761,
The coronal structure in August 1996 - A tomographic reconstruction

1996

Bentley,R.D. and Mariska,J.T. (eds.)1996, Astron.Soc.Pacific.Conf.Ser. Vol.111, San Francisco, California,
Magnetic reconnection in the solar atmosphere

Birk,G.T., Dreher,J., and Neukirch,T.1996, in Proc. Yohkoh Conference on Observations of Magnetic Reconnection in the Solar Atmosphere, Bath, England, March 20-22, 1996, (eds. R.Bentley and J.Mariska), Astron.Soc.Pac. Conf. Ser.111, p.89-94,
Three-dimensional numerical studies on coronal heating of X-ray bright points

D'Silva,S., Duvall,T.L., Jefferies,S.M., and Harvey,J.W.1996, ApJ 471, 1030-1043,
Helioseismic tomography

Demoulin,P., Mandrini,C.H., VanDriel-Gesztelyi,L., Priest,E.R., Henoux,J.C., and Schmieder,B.1996, in Proc. Yohkoh Conference on Observations of Magnetic Reconnection in the Solar Atmosphere, Bath, England, March 20-22, 1996, (eds. R.Bentley and J.Mariska), Astron.Soc.Pac. Conf. Ser.111, p.49-58,
3D magnetic reconnection: example of an X-ray bright point

Galsgaard,K., Rickard,G.J., Reddy,R.V., and Nordlund,A.1996, in Proc. Yohkoh Conference on Observations of Magnetic Reconnection in the Solar Atmosphere, Bath, England, March 20-22, 1996, (eds. R.Bentley and J.Mariska), Astron.Soc.Pac. Conf. Ser.111, p.82-88,

Dynamical properties of single and double 3D null points

Klimchuk,J.A.1996, in Proc. Yohkoh Conference on Observations of Magnetic Reconnection in the Solar Atmosphere, Bath, England, March 20-22, 1996, (eds. R.Bentley and J.Mariska), Astron.Soc.Pac. Conf. Ser.111, p.319-330,
Post-eruption arcades and 3-D magnetic reconnection

Mandrini,C.H., Demoulin,P., VanDriel-Gesztelyi,L., Schmieder,B., Cauzzi,G., Hofmann,A.1996, SP 168, 115-133,
3D magnetic reconnection at an X-ray bright point

Priest,E.R.1996, in Proc. Yohkoh Conference on Observations of Magnetic Reconnection in the Solar Atmosphere, Bath, England, March 20-22, 1996, (eds. R.Bentley and J.Mariska), Astron.Soc.Pac. Conf. Ser.111, p.331-340,
3D reconnection in complex topologies

Schmidt,W.K.H. and Bothmer,V.1996, Adv.Space Res. 17, 369-376,
Stereoscopic viewing of solar coronal and interplanetary activity

Schmidt,W.K.H. and others1996, A proposal to the European Space Agency for the next medium size mission (M3), ESA SP-1180, 116,
Lagrange: the sun and inner heliosphere in three dimensions

Winterhalter,D., Gosling,J.T., Habbal,S.R., Kurth,W.S., and Neugebauer,M.(eds.)1996, AIP COnf.Proc. Vol. 382, AIP PRess, Woodbury, New York,
Solar Wind Eight

Zidowitz,S., INhester,B., and Epple,A.1996, in Solar WInd Eight, (eds. WInterhalter, J.T.Gosling,S.R.Habbal, W.S.Kurth, and M.Neugebauer) pp.165-166, AIP COnf.Proc. 328, Woodbury, NY,
Tomographic inversion of coronagraph images

1995

Aschwanden,M.J.1995, Lecture Notes in Physics, 444, 13-34, Proc. CESRA workshop "Coronal Magnetic Energy Releases", Caputh/Potsdam, (eds. A.O.Benz and A.Krueger), Heidlberg:Springer,
Imaging, Stereoscopy, and Tomography of the Solar Corona in Soft X-rays and Radio

Aschwanden,M.J., Lim,J., Gary,D.E., and Klimchuk,J.A.1995, ApJ 454, 512-521,
Solar rotation stereoscopy in microwaves

Fushiki,T. and Sakai,J.I.1995, SP 161, 317-330,
3-D MHD simulation of the formation of spiral plasma flows during collision of two current loops

Fushiki,T. and Sakai,J.I.1995, SP 156, 265-280,
3-D MHD simulation of plasmoid formation during coalescence of two current loops

Jackson,B.V. and Froehling,H.R.1995, AA 299, 885-892,
Three-dimensional reconstruction of a coronal mass ejection

Sakai,J.I. and Fushiki,T.1995, SP 156, 281-292,
3-D MHD simulation of the generation of a shell current loop with closure current

1994

Aschwanden,M.J. and Bastian,T.S.1994, ApJ 426, 425-433,
VLA stereoscopy of solar active regions: I. method and tests

Aschwanden,M.J. and Bastian,T.S.1994, in Proc. Kofu Symp. on "New Look at the Sun with Emphasis on Advanced Observations of Coronal Dynamics and Flares'', eds. S.Enome and T.Hirayama, NRO Rep. No. 360, p.357-358,
VLA stereoscopy of solar active regions

Aschwanden,M.J. and Bastian,T.S.1994, ApJ 426, 434-448,
VLA stereoscopy of solar active regions: II. altitudes, relative motion, and center-to-limb darkening of 20 cm emission

Batchelor,D.A.1994, SP 155, 57-61,
Quasi-stereoscopic imaging of the solar X-ray corona

Davila,J.M.1994, ApJ 423, 871-877,
Solar tomography

Galsgaard,K. and Nordlund,A.1994, Space Sci.Rev. 68,
Dynamic behavior and topology of 3D magnetic fields

Jardine,M., Allen,H.R., and Grundy,R.E.1994, Space Sci.Rev. 68, 115-116,
The role of vorticity in 3D magnetic field annihilation

Molodensky,M.M., Starkova,L., and Koutchmy,S.1994, IAU Colloq. 144 on "Solar Coronal Structures", eds. V.Rusin, .Heinzel, and J.C.Vial, p.605-607,
A method to obtain stereo-diagrams of the solar disc

Poedts,S. and Goedbloed,J.P.1994, Space Sci.Rev. 68, 103-108,
3D nonlinear wave heating of coronal loops

Strong,K.T.1994, Chapter 3 of IACG report on Easton Workshop,
Studying the 3-D structure of large scale coronal features

1993

Davila,J.M.1993, NASA/GSFC report (1993 May 3), 66p,
The solar tomography mission: deducing the three dimensional structure of the solar corona

Hurlburt,N.E., Martens,P.C.H., Jaffey,S.M., and Slater,G.L.1993, AAS/SPD meeting, Stanford, California, July 13-16, 1993,
Computed tomographic reconstruction of the soft X-ray corona

Nishikawa,K., Sakai,J., Koide,S., Buneman,O., and Neubert,T.1993, in Proc. of 4th Internat.Conf. on Plasma Physics and Controlled Nuclear Fusion, ESA SP-351, p.229-232,
Current loop coalescence studied by 3-D electromagnetic particle code

1992

Aschwanden,M.J., Bastian,T.S. and White,S.M.1992, ESA SP-348, p.217, Proc. First SOHO workshop, 25-28 Aug 1992, Annapolis/MD
3D reconstruction methods of coronal structures by radio observations

Davila,J.M. and Thompson,W.T.1992, ApJ 389, L91-L93,
A rotating tomographic imager for solar extreme-ultraviolet/soft X-ray emission

Kane,S.R., McTiernan,J., Loran,J., Fenimore,E.E., Klebesadel,R.W., and Laros,J.G.1992, ApJ 390, 687-702,
Stereoscopic observations of a solar flare hard X-ray source in the high corona

Koutchmy,S., and Molodensky,M.M.1992, Nature 360, 717,
Three-dimensional image of the solar corona from white-light observations of the 1991 eclipse

1991

Sakai,J.I. and DeJager,C.1991, SP 134, 329,
High-energy flare explosions driven by 3-dimensional X-type current loop coalescence

1988

Deutsch,M., Notea,A., and Pal,D.1988, Applied Optics, 27/19, 3692,
Reconstruction of discontinuous density profiles of cylindrically symmetric objects from single x-ray projections

Ravichandran,M., and Gouldin,F.C.1988, Applied Optics 27, No.19, 4084,
Reconstruction of smooth distributions from a limited number of projections

Stark,H., and Peng,H.1988, J.Opt.Soc.Am.A 5, No.3, 331,
Shape estimation in computer tomography from minimal data

1986

Gull,S.F., and Newton,T.J.1986, Applied Optics, 25/1, 156,

Maximum entropy tomography

1985

Berton,R. and Sakarai,T.1985, SP 96, 93-111,
Stereoscopic determination of the three-dimensional geometry of coronal magnetic loops

Beylkin,G.1985, Applied Optics, 14, No. 23, 4086,
Reconstruction discontinuities in multidimensional inverse scattering problems: smooth errors vs small errors

Dhawan,P., Rangayyan,R.M., Gordon,R.1985, Applied Optics 24, No.23, 4013,
Image restoration by Wiener deconvolution in limited-view computed tomography

Frieden,B.R., and Zoltani,C.K.1985, Applied Optics, 24/No.23, 3993,
Maximum bounded entropy: application to tomographic reconstruction

Hanson,K.M. and Wecksung,G.M.1985, Appl.Optics 24, No.23, 4028,
Local basis-function approach to computed tomography

Heffernan,P.B., and Robb,R.A.1985, Applied Optics 24, No.23, 4105,
Difference image reconstruction from a few projections for nondestructive materials inspection

Rangayyan,R., Dhawan,A.P., and Gordon,R.1985, Applied Optics 24, No.23, 4000,
Algorithms for limited-view computed tomography: an annotated bibliography and a challenge

Schwenn,R.1985, in Proc. of 19th ESLAB Symposium, Les Diablerets, Switzerland, (Dordrecht:Reidel), in "Astrophysics and Space Science Libray",
Relationship of coronal transients to interplanetary shocks: 3D aspects

1983

Byrne,C.L., Fitzgerald,R.M., Fiddy,M.A., Hall,T.J., and Darling,A.M.1983, J.Opt.Soc.Am. Vol.73, No. 11, 1481,
Image restoration and resolution enhancement

Censor,Y.1983, Proc.IEEE 71, No.3, 409,
Finite series-expansion reconstruction methods

Hanson,K.M., and Wecksung,G.W.1983, Opt.Soc.Am., 73, No.11, 1501,
Bayesian approach to limited-angle reconstruction in computed tomography

Lewitt,R.M.1983, Proc.IEEE 71/3, 390,
Reconstruction algorithms: transform methods

Medoff,B.P., Brody,W.R., Nassi,M., and Macovski,A.1983, J.Opt.Soc.Am. 73, No.11, 1493,
Iterative convolution backprojection algorithms for image reconstruction from limited data

Udupa,J.K.1983, Proc. IEEE 71, No.3, 420,
Display of 3D information in discrete 3D scenes produced by computerized tomography

1981

Barrett,H.H. and Swindell,W.1981, Academic Press:New York,
Radiological imaging. The theory of image formation, detection, and processing

Lahart,M.J.1981, J.Opt.Soc.Am. 71, No.10, 1155,
Estimation of reconstructions in computed tomography

Tam,K.C., and Perez-Mendez,V.1981, J.Opt.Soc.Am. 71, No.5, 582,
Tomographical imaging with limited-angle input

1980

Frieden,B.R.1980, Computer Graphics and Image Processing 12, 40-59,
Statistical models for the image restoration problem

1979

Altschuler,M.D.1979, in Image Reconstruction from Projections, (ed. G.T.Herman, Berlin:Springer, p.105-145, (GSFC TA 1632.I415)
Reconstruction of the global-scale three-dimensional solar corona

Chiu,M.Y., Barrett,H.H., Simpson,R.G.1979, J.Opt.Soc.Am. 70, No.7, 755,
Three-dimensional reconstruction from planar projections

Chiu,M.Y., Barrett,H.H., Simpson,R.G., Chou,C., Arendt,J.W., and Gindi,G.R.1979, J.Opt.Soc.Am. 69, No.10, 1323,
Three-dimensional radiographic imaging with a restricted view angle

Kramer,D.M. and Lauterbur,P.C.1979, IEEE Trans Nucl.Sci. Vol. NS-26, No.2,
On the problem of reconstructing images of non-scalar parameters from projections

Minerbo,G.1979, Computer graph. and Image Proc. 10, 48-68,
MENT: A maximum entropy algorithm for reconstructing a source from projection data

1978

Das,Y., Boerner,W.M.1978, IEEE Trans.Antennas and Propagation, Vol.AP-26, No.2, 274,
On radar target shape estimation using algorithms for reconstruction from projections

1977

Swindell,W., and Barrett,H.H.1977, Physics Today, Dec.1977, 32,
Computerized tomography: taking sectional x rays

1974

Garroway,A.N.1974, J.Phys.D., Appl.Phys. 7, L159,
Velocity measurements in flowing fluids by MNR

1973

Smith,P.R., Peters,T.M., and Bates,R.H.T.1973, J.Phys. A. Math.Nucl.Gen. 6, 361
Image reconstruction from finite numbers of projections

Source: aschwanden@lmsal.com